



Helianthus tuberosus as a promising feedstock for bioenergy and chemicals appraised through pyrolysis, kinetics, and TG-FTIR-MS based study



Muhammad Aamer Mehmood^{a,b}, Muhammad Sajjad Ahmad^b, Qian Liu^a, Chen-Guang Liu^{a,*},
Mudassir Hussain Tahir^c, Akram Ahmed Aloqbi^d, Nasrin Ibrahim Tarbiah^d,
Hadeil Muhanna Alsufiani^e, Munazza Gull^e

^a State Key Laboratory of Microbial Metabolism, Joint International Research Laboratory of Metabolic & Developmental Sciences of Ministry of Education, School of Life Science and Biotechnology, Shanghai Jiao Tong University, Shanghai 200240, China

^b Department of Bioinformatics and Biotechnology, Government College University Faisalabad, Faisalabad 38000, Pakistan

^c Department of Polymer Science and Engineering, University of Science and Technology of China, 96 Jinzhai Road, Hefei, Anhui Province 230026, China

^d Biology Department, University of Jeddah, Saudi Arabia

^e Biochemistry Department, King Abdul Aziz University, Jeddah, Saudi Arabia

ARTICLE INFO

Keywords:

Jerusalem artichoke
Waste biomass
Pyrolysis
TG-FTIR-MS
Bioenergy
Chemicals

ABSTRACT

The Jerusalem artichoke (*Helianthus tuberosus*) is a perennial plant which is adapted to wide climatic conditions ranging from temperate to semiarid regions. Its tubers are alternative to potatoes and it can typically produce 18–28 tons of waste foliage from one hectare which can be exploited for bioenergy via pyrolysis. However, the pyrolytic behavior of its waste was never studied. The present study was focused to assess its potential via pyrolysis, kinetics, thermodynamics, and TG-FTIR-MS based study to produce energy and chemicals. The biomass was subjected to thermal degradation at five heating rates (10, 20, 30, 40, 80 °C/min) under an inert environment. The thermograms showed that the highest rate of thermal transformation was achieved at 270–430 °C. The data were subjected to kinetics and thermodynamics analyses using Kissinger-Akahira-Sunose (KAS), Flynn-Wall-Ozawa (FWO), Starink and Vyazovkin models. The activation energy (E_a) and pre-exponential factors remained consistent and ranged from 160 to 175 kJ/mol and 10^{12} – 10^{14} s⁻¹ at conversion fractions ranging from $\alpha = 0.2$ to $\alpha = 0.6$. The kinetic parameters showed higher statistical confidence with $R^2 \geq 0.98$ and good agreement among the data obtained through various models. The high heating value (HHV = 18.76 MJ/kg), change in enthalpy ($\sim \Delta H = 150$ – 170 kJ/mol), and Gibbs free energy ($\Delta G = 158$ – 168 kJ/mol) demonstrated the substantial bioenergy potential of this waste. Moreover, the pyrolytic gases were subjected to Thermogravimetric-Fourier Transformed Infrared Spectroscopy-Mass Spectrometry (TG-FTIR-MS) analyses to identify the nature of products. The detected functional groups showed that the evolved gases contained aldehydes, phenols, carboxylic acids, esters, aromatic hydrocarbons and methane which indicated the substantial potential of this waste to produce energy and chemicals via pyrolysis causing no competition with the food/feed or land for food/feed.

1. Introduction

Increased global mobility, heavy industrialization and excessive burning of petroleum-derived chemicals caused the emission of toxic and greenhouse gases (CO₂, SO_x, NO_x). Besides environmental issues, ever-increasing demands of liquid fuels cannot be fulfilled in the next 50–70 years, hence finding the environmentally sustainable alternative liquid fuels would be inevitable. Biomass, along with solar and wind, has shown to be the most promising foreseeable source to fuel the future due to its renewable and carbon neutral nature [1]. Biomass can be

obtained from various sources but the use of residual biomass from agricultural or agroforestry and the biomass produced on non-arable lands would be a practical choice without causing any direct or indirect competition with the food or land for food [2]. The photosynthetic storage of solar energy into biomass is 58–90 folds higher when compared to the storage capacity of lithium-ion (Li-ion) batteries on mass basis [1]. However, the photosynthetically stored energy in biomass is difficult to retrieve when compared to the retrieval from Li-ion batteries.

Several methods can be employed for the cleaner conversion of

* Corresponding author.

E-mail address: cg.liu@sjtu.edu.cn (C.-G. Liu).

biomass to energy and chemicals ranging from direct combustion to thermochemical and biological fermentation. Although biological fermentation is the cleanest way to convert biomass into renewable fuels, yet the recalcitrance nature of biomass and tedious methodology involved makes the process overall inefficient and expensive. Moreover, thermochemical conversion has dominance over biological methods in terms of conversion efficiency [3]. Pyrolysis is the thermal conversion of biomass into energy, gases, biooil, biochar and chemicals under inert environment [4] which has shown to be another cleanest method to retrieve the energy stored in the plant biomass leaving almost no waste at the end. While, the process itself is affected by several factors including nature of the biomass, temperature, heating rate, particle size of the biomass and resident time. For instance, the higher oxygen content in the biomass indicates the capability of biomass to produce high-value gases, liquid fuels and better-quality biochar [5]. Similarly, the presence of water vapors during the pyrolysis process can increase the proportion of liquid products. Moreover, porosity and surface area will influence the biochar formation using simultaneous pyrolysis and gasification [4]. Hence, establishing effective pyrolysis for any biomass requires a vibrant understanding of the key parameters involved.

Thermogravimetry is extensively employed to monitor the thermal conversion of biomass through pyrolysis, combustion, and gasification in response to a gradually increasing temperature in a thermogravimetric analyzer (TGA). The data obtained provide information on the decomposition rate of biomass as a function of time and temperature in a controlled environment which is maintained as inert during pyrolysis. Moreover, the data are subjected to mathematically derived models to establish the reaction kinetics which subsequently elucidate the feasibility and behavior of the pyrolytic behavior of the biomass under study [6]. The data analyses reveal kinetics and thermodynamic parameters of the pyrolysis process, including Gibb's free energy, enthalpy of the reaction, activation energy, and pre-exponential factors. There are two common approaches based on mathematical modeling namely model free (isoconversional) and model fitting methods which are often used to calculate the kinetic parameters. Where it is required to assume a model while using fitting approach opposite to model free methods where the assumption is not necessary. Thus, model-free methods are taken as more reliable [7,8]. Model-free methods include Kissinger-Akahira-Sunose (KAS), Ozawa-Flynn-Wall (OFW), Starink and Vyazovkin which are broadly accepted as reliable techniques to compute kinetic parameters.

The pyrolysis of biomass releases gases where nature and composition of the products are often monitored using thermogravimetry (TG) coupled with a Fourier transform infrared (FTIR) and/or Mass spectrometer in real-time. TG-FTIR or TG-FTIR-MS systems enable us to monitor the type and proportion of the volatiles produced during the pyrolysis [9,10] and/or co-pyrolysis [11,12]. Previously, several studies have been conducted to understand the pyrolytic behavior of several residual biomasses including sawdust [13], rice husk, [14], tobacco waste [15], red pepper waste [8], walnut shells [16], Pea waste [17], Chinese liquor industry waste [18], tea waste [19] and raw coal [20]. These studies have shown the remarkable potential of the studied residual biomass to produce energy, fuel, and chemicals in cost and energy efficient way.

Other than pyrolysis parameters, cost of feedstock is the key parameter which influences the cost-effectiveness of the process while the price of biomass depends on the inputs provided, the value of land used, and type of the biomass produced. For instance, miscanthus and willow are established bioenergy crops, which costs US\$ 12–26 per GJ of energy, when subjected to pyrolysis [21]. In this scenario, one strategy to lower the cost of production is to utilize the residual or waste biomass using the grasses adapted to non-arable lands which can turn these non-profitable lands into profitable future energy landscapes without causing any direct competition with food crops or land for food crops [2].

The Jerusalem artichoke (*Helianthus tuberosus*) is a herbaceous

perennial plant which grows to 1.5–3.0 m tall, where its underground tubers are used a vegetable as an alternative of potato. Typically, it can produce 16–20 tons of tubers along with 18–28 tons of foliage from one hectare of land ranging from temperate regions of North America to semiarid regions of China. Unlike other tubers, the tubers of Jerusalem artichoke contain inulin as the main sugar molecule which is not easily digestible by a human. Alternatively, its carbohydrates can be converted to ethanol fuel using yeast strains capable of inulin fermentation. This plant is easy to cultivate due to its dominant, invasive, and adaptive nature. These features make the foliage of Jerusalem artichoke as an abundantly available, low-cost waste biomass to produce energy and chemicals. Previously, the basic pyrolysis of its tubers was studied using distribution activation energy model [22]. In the present study, the whole plant biomass of this plant (except tubers) was subjected to pyrolysis, kinetics, thermodynamics, and TG-FTIR-MS based study to evaluate its potential for energy and chemicals for the very first time. The data have shown that Jerusalem artichoke biomass has the remarkable potential to produce chemicals and energy via pyrolysis.

2. Materials and methods

2.1. Sample collection, proximate and elemental composition analyses

The residual biomass of Jerusalem artichoke plant after harvesting the tubers for food purpose was collected from Jiangsu Province of China. The plant biomass was cleaned using tap water to remove any soil particles and was left under the sun for air drying. Later, the whole plant was chopped down to reduce the size for easy storage and handling. A known mass of the sample was exposed to 105 °C for 48 h in a hot air oven. The oven-dried biomass was finely grounded using a blender and mass was passed through a strainer to collect the powdered biomass of particle size ranging from 200 to 250 μm to ensure the uniform heat transfer during thermal degradation in pyrolysis. The powder-like biomass was kept in a desiccator for further experiments. Proximate analyses namely volatile content (VM), moisture content and ash content were estimated using previously established standard methods in ASTM (E872-82 2006, E871-82 2006, E1755-01 2007). Where a known mass of air-dried sample was placed in a hot-air oven at 105 °C in triplicate unless a constant mass was attained. The difference in mass before and after 105 °C treatment gave the moisture content. Similarly, the pre-determined mass was taken into ceramic crucibles and put at 550 °C in a Muffle furnace for 4 h. Where the difference in mass before and after heating gave the volatile matter content and the residual mass in the crucible was considered as ash. The oven-dried biomass was used to determine the high calorific value using an Oxygen Bomb calorimeter following the GBT 213-2008 test standards. The composition of major elements namely oxygen, nitrogen, sulfur, hydrogen and carbon were assessed using Vario EL Cube elemental analyzer (Germany) using Argon as a carrier gas.

2.2. Thermogravimetric (TG) and TG-FTIR-GCMS analyses

Almost 10.0 mg of finely divided oven-dried biomass was taken in aluminum crucibles and subjected to five different thermal degradation experiments at five different heating rates including 10, 20, 30, 40, and 80 °C/min starting from 25 °C to 1000 °C in a thermogravimetric analyzer STA-409 (NETZSCH-Gerätebau GmbH, Germany). While 100 mL/min flow rate of nitrogen was maintained to ensure the inert environment in the reaction chamber.

After the thermogravimetric experiments, the same amount of oven-dried powdered biomass was subjected to thermal degradation at the heating rate of 40 °C/min in a Thermogravimetric-Fourier Transformed Infrared Spectroscopy coupled with Gas Chromatography-Mass Spectrometer (TG-FTIR-GC-MS) to monitor the major pyrolytic products during thermal degradation. Where an initial temperature of 115 °C was upheld for 10 min to ensure the removal of entrapped

moisture. Later, the biomass was degraded at a constant heating rate of $40\text{ }^{\circ}\text{C min}^{-1}$ and the evolved gases were analyzed using the detectors present in the FTIR. The GCMS analysis of the evolved gases was performed using positive electron impact (EI) ionization mode at 70 eV. While an initial temperature of $50\text{ }^{\circ}\text{C}$ was maintained in the oven for 3 min then was ramped to $400\text{ }^{\circ}\text{C}$ at the rate of $40\text{ }^{\circ}\text{C/min}$ and was maintained for 5 min. The temperature of the injector was set at $150\text{ }^{\circ}\text{C}$, while temperatures of the transfer line and ion source were set at $50\text{ }^{\circ}\text{C}$. Different components of the sample were separated by the TR-5MS column ($30\text{ m} \times 250\text{ }\mu\text{m}$) using (He) as the carrier gas.

2.3. Establishing the mathematical model for the data analyses

The TGA data is often analyzed using the model-free (isoconversion) methods. These methods are based on the Arrhenius Equation. The equation for isoconversion methods is written as given below;

$$\frac{d\alpha}{dt} = f_1(T)f_2(\alpha) \quad (1)$$

where $f_1(T)$ is the temperature dependency (Arrhenius equation), and $f_2(\alpha)$ is the conversion function. The Eq. (1) was reproduced as $f_1(T)$ which be contingent on the temperature.

$$\frac{d\alpha}{dt} = k(T)f_2(\alpha) \quad (2)$$

$$\alpha = (m_o - m_i)/(m_o - m_{\infty})$$

According to the Arrhenius equation

$$k(T) = A \exp\left(-\frac{E}{RT}\right) \quad (3)$$

After substituting Eq. (3) into Eq. (2), Eq. (4) was obtained.

$$\frac{d\alpha}{dt} = A \exp\left(-\frac{E}{RT}\right) f_2(\alpha) \quad (4)$$

$$\beta = \frac{dT}{dt},$$

So, Eq. (4) became as follows:

If the differential coefficient mechanism function is written in general nth order form as follows,

$$f_2(\alpha) = (1 - \alpha)^n \quad (5)$$

Then Eq. (4) can be written in a general way as:

$$\frac{d\alpha}{dT} = \frac{A}{\beta} \exp\left(-\frac{E}{RT}\right) (1 - \alpha)^n \quad (6)$$

Now, if Eq. (6) is integrated for first reaction order and for the initial conditions, $\alpha = 0$, at $T = T_0$, to obtain the following expression:

$$G(\alpha) = \int_0^{\alpha} d\alpha / f_2(1 - \alpha) = (A/\beta) \int_{T_0}^T \exp(-E/RT) dT \\ = (AE/\beta R) \mathbf{p}(-E/RT) \quad (7)$$

After some mathematical manipulations following equation were obtained that was further used to develop models.

$$G(\alpha) = (ART^2/\beta E [1 - 2RT/E]) \exp(-E/RT) \quad (8)$$

Rearranging Eq. (8) it was identified that the “ $2RT/E_a$ ” was negligible when compared to unity and was ignored (Coats, 1964), accordingly, the following equation was obtained.

$$G(\alpha) = (ART^2/\beta E) \exp(-E/RT) \quad (9)$$

2.4. Models employed

Three models namely KAS [23–25], Starink [26] and FWO [24] were employed to calculate kinetic parameters.

$$\ln\left(\frac{\beta}{T^2}\right) = \ln(AR/EG(\alpha)) - E/RT \quad \text{KAS} \quad (10)$$

$$\ln\left(\frac{\beta}{T^{1.92}}\right) = \ln(AR/EG(\alpha)) - E/RT \quad \text{Starink} \quad (11)$$

$$\ln\beta = \ln(AE/RG(\alpha)) - E/RT \quad \text{FWO} \quad (12)$$

$$\ln\left(\frac{g(\alpha)}{T^2}\right) = \ln\left(\frac{AR}{\beta E_a}\right) - \frac{E_a}{RT} \quad \text{Coats - Redfern} \quad (13)$$

Then, the left-hand sides of the Eqs. (10)–(12) were plotted against the inverse of pyrolysis temperature. Then, for any selected α value, the kinetic parameters were calculated from the value of the slope and intercept. The Pre-exponential factors were also determined through the recommendations devised by ICTAC kinetic committee by using the compensation effect [27]. However, these values were estimated on each conversion point (α) using the following standard equations that have already proposed by ICTAC standards protocols.

$$\ln(A)_i = aE_{ai} + b \quad (14)$$

Moreover ΔH , ΔG and ΔS were calculated with standard equation.

$$\Delta H = E - RT \quad (15)$$

$$\Delta G = E + RT_m \ln(K_B T_m/hA) \quad (16)$$

3. Results and discussion

3.1. Physicochemical properties assessed via proximate and ultimate analyses

Elemental analysis of the whole plant biomass of Jerusalem Artichoke (without tubers) showed to contain 43.56–43.62% C, 5.35–5.40% H, 47.48–47.58% O, 0.49–0.51% N, and < 0.10% S. Although these values were approximately in accordance with most of the plant biomass sources overall sample showed extremely low S and N content which indicates the suitability of this biomass for combustion and pyrolysis. Because lower N and S content will release the least amount of the noxious and soxious gases upon combustion or pyrolysis. While a considerably higher proportion of C, H, and O indicates the feasibility to produce energy, syn-gases and biooil because it is the organic content which goes into pyrolytic products upon thermal degradation. Consistently, the 70.42% of volatile matter, 3.25% moisture, 8.85% ash, 17.48% fixed carbon content again reflected the suitability of the sample to produce syngases and biooil via thermal degradation. Because, the biomass with moisture content < 10%, nitrogen < 2.0% and sulfur content < 0.2% is considered as suitable for pyrolysis [16]. The High Heating Value (HHV) of the biomass was shown to be 18.76 MJ/kg which is remarkably high when compared to the HHV values of established energy crops and other perennial grasses including Giant reed (17.20 MJ/kg), Willow (17.80 MJ/kg), Reed canarygrass (17.80 MJ/kg), Para grass (15.04 MJ/kg), Camel grass (15.00 MJ/kg) [28–31]. In conclusion, the physicochemical properties of the residual biomass of Jerusalem Artichoke plant show the remarkable bioenergy potential of this low-cost feedstock.

3.2. Thermal degradation behavior assessed through TG-DTG curves

Pyrolysis experiment of Jerusalem Artichoke (JA) was performed at five heating rates to observe the thermal degradation pattern for product formation as shown in Fig. 1. It was shown that different heating rates affected the thermal degradation gently, as shown by the slight shift of TG curves between 270 and 430 $^{\circ}\text{C}$ while major mass loss occurred during this temperature range. Similar tilt was previously observed in the TG-curves of date palm waste, olive mill waste, *Tecktona grandis* and non-woody lignocellulose biomass [32–35] which reflects

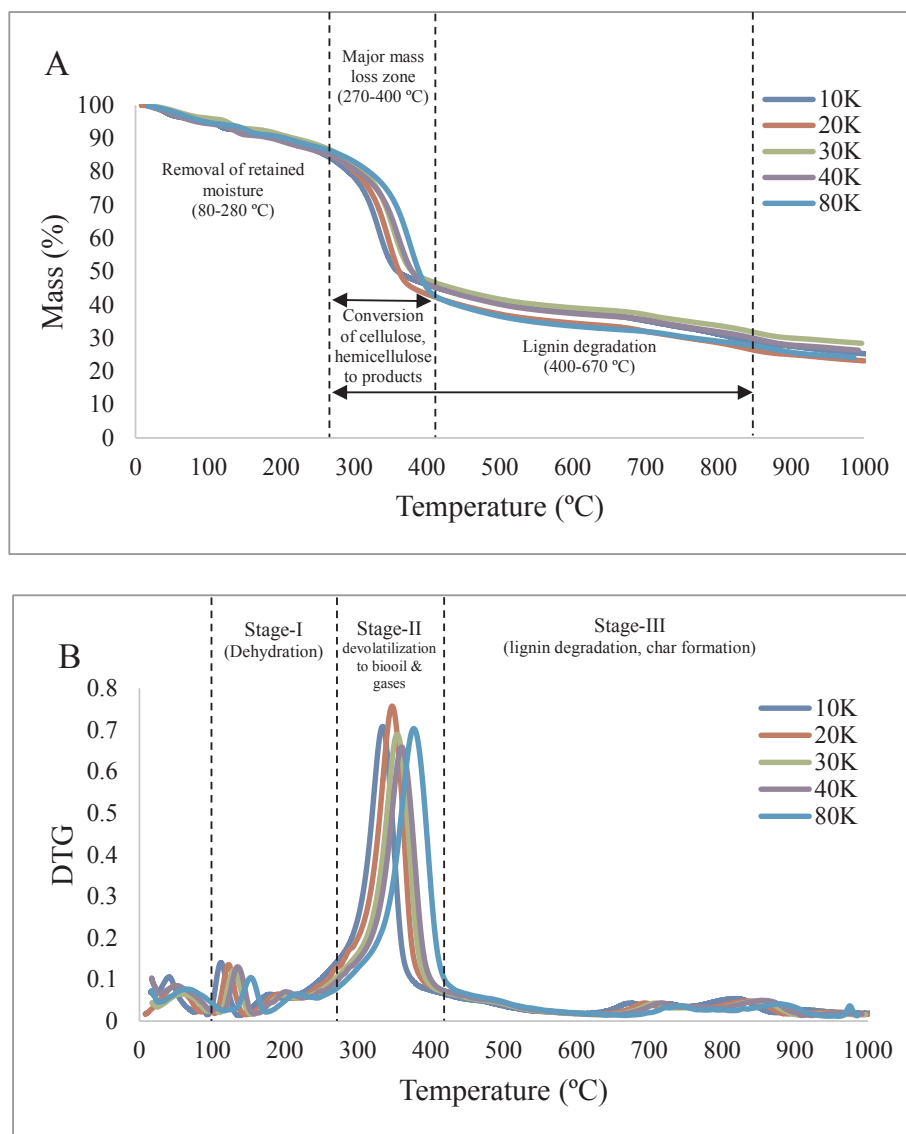


Fig. 1. TG pattern of JA (A). DTG Pattern of JA (B) under heating rates (10, 20, 30, 40 and 80) K min⁻¹.

Table 1

Characteristics temperatures associated with the pyrolysis reaction of JA biomass.

Heating rate (°C min ⁻¹)	Temperature (°C), Stage-II		
	(Starting Temperature) T_1	(Peak Temperature) T_2	(Ending Temperature) T_3
10	177	332	380
20	185	347	390
30	195	353	397
40	178	360	406
80	174	376	424

that either the heating rate have little influence on the product formation pattern or it is due to the rate of heat transfer into the biomass. The characteristic temperatures associated with the thermal conversion of biomass are shown in Table 1. Moreover, the thermal degradation pattern of the JA was shown to occur in three distinct stages (Table 2). The first stage was observed when the temperature was increased from ambient (25 °C) to T_1 (174–178 °C) where 8.65–9.4% loss in mass was observed. This loss in mass indicates the removal of retained moisture in cellular/intracellular compartments and adsorbed on the surface.

Table 2

Thermal degradation stages of JA biomass at different heating rates.

Stages	Temperature Ranges	Heating rate (°C min ⁻¹)				
		10	20	30	40	80
Stage-I, Mass Loss (%)	$T_{min}-T_1$	9	9	8.5	8.5	9.8
Stage-II, Mass Loss (%)	T_1-T_3	62	60	63	60.71	58.35
Stage-III, Mass Loss (%)	T_3-T_{max}	47	44	47.7	45.64	41.40
Final residues at 1000 °C (%)		25.07	23	28.5	26.17	23.97

Where the biomass with retained moisture $\leq 10\%$ is considered as valuable for pyrolysis and combustion [14]. The second stage occurred between 270 °C and 430 °C which should be referred as devolatilization stage where most of the product formation occurred. A variety of volatiles would have been released during this stage resulting in a drastic mass loss from 43.4% to 50.08% at 10 °C/min to 80 °C/min. This finding is in accordance with the reported temperature range for the thermal degradation of hemicellulose (220–300 °C), cellulose (300–340 °C), and lignin (> 340 °C) [36]. Major mass loss during this stage indicates that most of the pyrolytic products can be obtained below 270–430 °C. During the third stage, degradation of lignin

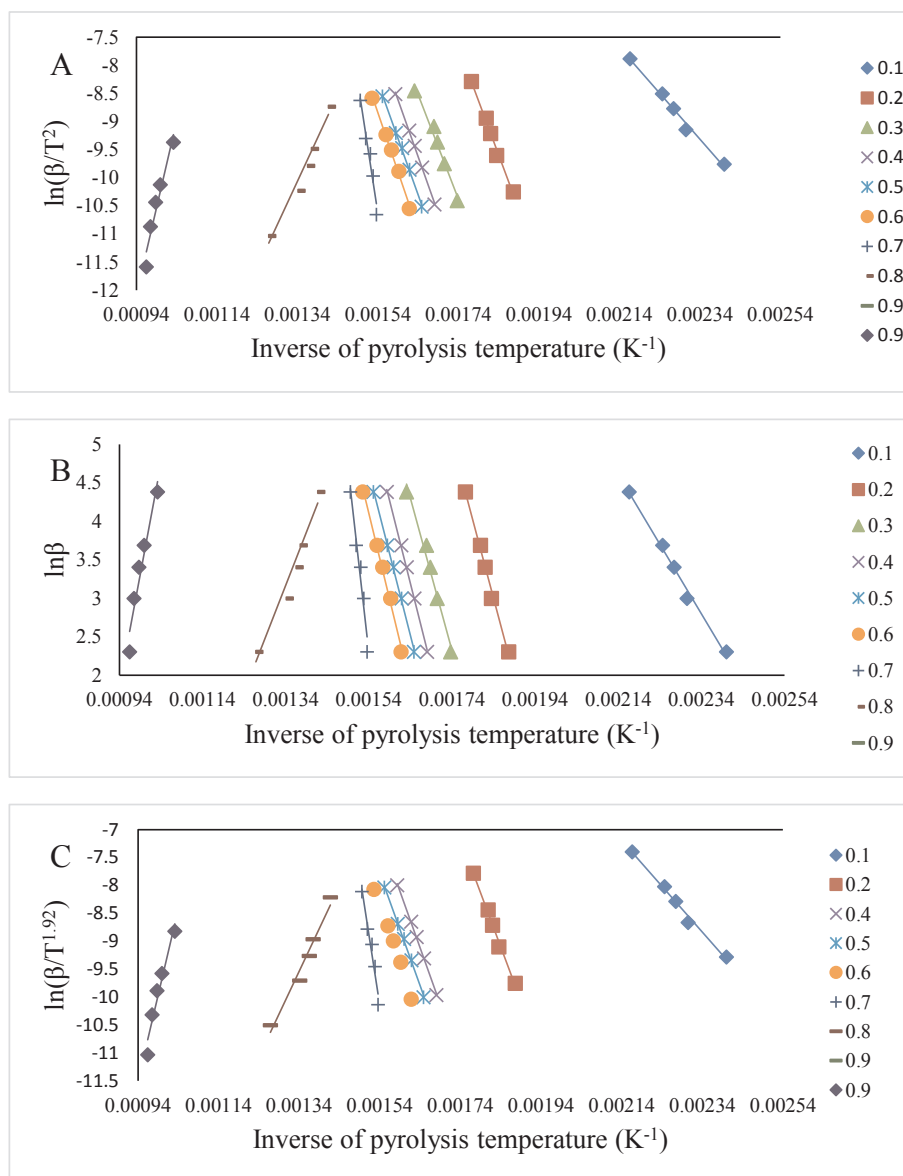


Fig. 2. Regression lines of JA to calculate activation energy values for KAS, FWO and Starink.

component and charring was the main event which occurred at the temperature ranging from 430 to 700 °C followed by a tail up to 1000 °C. Approximately 16–23% of the mass was lost during the third stage which mainly indicates the decomposition of residual lignin. Where, lignin contributes towards biochar production thermal stability [14,33]. Final residues ranged from 23 to 28.5% at 1000 °C which indicated the substantial char formation making the JA biomass for considerable biochar production as a side-product of the pyrolysis process.

3.3. Reaction kinetics and activation energy of pyrolysis

Linear fit plots were obtained by plotting either $\ln\left(\frac{\beta}{T^2}\right)$, $\ln\beta$, or $\ln(\beta/T^{1.92})$ on Y-axis against the inverse of pyrolysis temperature ($1/T$) on X-axis (Fig. 2). Energy values were obtained through three isoconversion methods KAS, FWO and Starink which reinforced each other when results were compared (Table 3). The E_a -values obtained from all the methods were consistent to each other on each conversion (α) which confirmed accuracy of the experimental data with $R^2 \geq 0.98$. The E_a values were ranging from 67 to 388 kJ/mol

(Avg. 185 kJ/mol), 71.54–379 kJ/mol (Avg. 180 kJ/mol), and 68–388 kJ/mol (Avg. 185 kJ/mol) determined by KAS, FWO, and Starink methods for conversion (α) ranging from 0.1 to 1.0. To ensure the reliability of data, the E_a values obtained from all methods were compared for the conversion (α) ranging from 0.2 to 0.8, because the values obtained at too low ($\alpha < 0.2$) or too high conversion points ($\alpha > 0.8$) may contain errors because at these values thermal degradation does not reflect the overall pyrolytic behavior [37]. From the comparison (Fig. 3) it was shown that E_a values almost remained consistent (160–175 kJ/mol) from conversion $\alpha = 0.2$ –0.6 while a sharp rise in activation energy was observed for $\alpha = 0.7$ which indicates the change of reaction chemistry. This rise in E_a value may be correlated with the initiation of lignin degradation which absorbed more energy due to its resilient structure. Moreover, the E_a value at $\alpha = 0.7$ was 379–388 kJ/mol, which was the highest when compared to the E_a values at other conversion points which again reflects that some highly endothermic reaction occurred at this stage. Moreover, comparison of E_a values of the JA sample with several other feedstocks indicated the suitability of JA biomass for energy efficient pyrolysis and co-pyrolysis with agricultural residues [38], rice husk [14], canola residues [39], banana peel waste [40] and horse manure [41].

Table 3
Kinetics and thermodynamics parameters.

α	E_a kJ/mol	R^2	A s^{-1}	ΔH kJ/mol	ΔG kJ/mol	ΔS J/mol
<i>KAS method</i>						
0.1	67.95	0.99	1.38E-01	62.8	233.50	-275.76
0.2	159.64	0.99	2.22E+12	154.49	168.69	-22.93
0.3	154.66	0.98	4.26E+11	149.51	172.21	-36.66
0.4	168.18	1.00	3.78E+13	163.04	162.66	0.62
0.5	166.62	1.00	2.25E+13	161.47	163.76	-3.69
0.6	174.69	0.99	3.27E+14	169.54	158.05	18.57
0.7	387.81	0.96	1.63E+45	382.67	7.42	606.22
0.8	127.74	0.96	5.65E+07	122.59	191.23	-110.89
0.9	257.25	0.94	2.55E+26	252.11	99.70	246.22
Avg.	185	1.00	-	179.8	150.80	-
<i>FWO method</i>						
0.1	71.54	0.99	4.54E-01	66.40	230.96	-265.86
0.2	160.47	0.99	2.93E+12	155.32	168.10	-20.64
0.3	156.48	0.98	7.80E+11	151.33	170.92	-31.65
0.4	169.55	1.00	5.95E+13	164.40	161.68	4.39
0.5	168.34	1.00	3.98E+13	163.19	162.54	1.06
0.6	176.18	0.99	5.36E+14	171.03	157.00	22.67
0.7	379.22	0.96	9.43E+43	374.08	13.49	582.53
0.8	109.65	0.97	1.40E+05	104.50	204.02	-160.77
0.9	228.79	0.95	2.03E+22	223.65	119.81	167.74
Avg.	180	1.00	-	174.9	154.28	-
<i>Starink method</i>						
0.1	68.24	0.99	1.52E-01	63.23	228.89	-274.74
0.2	160	0.99	2.51E+12	154.99	168.08	-21.72
0.3	155.05	0.98	4.85E+11	150.04	171.37	-35.37
0.4	168.59	1.00	4.33E+13	163.57	162.39	1.96
0.5	167.04	1.00	2.59E+13	162.03	163.42	-2.31
0.6	175.1	0.99	3.75E+14	170.09	158.08	19.91
0.7	388.25	0.96	1.88E+45	383.24	16.82	607.65
0.8	127.24	0.97	4.79E+07	122.23	189.79	-112.05
0.9	256.58	0.95	2.04E+26	251.57	104.08	244.59
Avg.	185.12	0.98	-	180.1	151.44	-

3.4. Thermodynamics parameters

The thermodynamic parameters including pre-exponential values ($A s^{-1}$), enthalpy change (ΔH kJ/mol), Gibb's free energy (ΔG kJ/mol) and change in entropy (ΔS kJ/mol) indicate the pyrolysis behavior of the sample under study. While these parameters are better calculated at lower heating rates [41] for this reason all these parameters were calculated at a heating rate of $10^\circ C/min$.

3.4.1. Pre-exponential factors (A, s^{-1})

The values of pre-exponential factors at $\alpha = 0.2-0.6$ were ranging from 10^{11} to 10^{14} obtained by KAS, FWO and Starink method which reflects that best reaction chemistry is described (Table 3). Similarly, the pre-exponential value of $10^{43}-10^{45}$ was obtained at the $\alpha = 0.7$ which happened due to extra energy required to initiate the lignin degradation because higher pre-exponential value indicates higher collisions which require more energy. Later, the pre-exponential value was dropped to $10^{05}-10^{07}$ at $\alpha = 0.8$. Similarly, higher activation energy and the higher pre-exponential value were observed at $\alpha = 0.7$ for the horse manure pyrolysis [41] which was dropped to normal at $\alpha = 0.8$. Moreover, a wide range of the pre-exponential values indicates the change in reaction chemistry and product formation with the changing conversional fractions which has been observed previously for the pyrolysis of cattle manure [42], *Typha latifolia* [43], Chinese liquor industry waste [18] and *Wolffia arrhiza* [44].

3.4.2. Change in enthalpy ($\Delta H, kJ/mol$)

Enthalpy change (ΔH kJ/mol) reflects the amount of energy involved in the formation of the activated complex. The ΔH values are a measure of the difference of energy between the reactants and the activated complex. While lower difference indicates that activated complex and product formation is being thermodynamically favored. The enthalpy values of JA biomass pyrolysis were observed ranging from 149 to 169 kJ/mol, 151–163 kJ/mol, and 150–170 kJ/mol at $\alpha = 0.2-0.6$, obtained by KAS, FWO and Starink methods respectively, with an approximate difference of ~ 5 kJ/mol with the E_a -values at the same conversional fractions. This difference was maintained throughout the process of thermal transformation which demonstrated that the product formation was easy energy efficient. Moreover, the ΔH values calculated by KAS, FWO, and Starink models were in consistency with each other at all conversional fractions (Fig. 4), which reflect the reliability of the data.

3.4.3. Gibbs free energy ($\Delta G, kJ/mol$)

The Gibbs free energy (ΔG , kJ/mol) indicate the amount of energy which could become available from the pyrolysis of a sample under study. The increasing difference in Gibbs free energy is a positive reflection to produce energy from the biomass pyrolysis. The ΔG values varied from 167 to 158 kJ/mol at $\alpha = 0.2-0.6$ and these values were consistent with each other obtained from KAS, FWO and Starink models which indicates a constant energy output from the pyrolysis of JA biomass at these conversional fractions. Moreover, this available energy was higher when compared to the ΔG of the horse manure

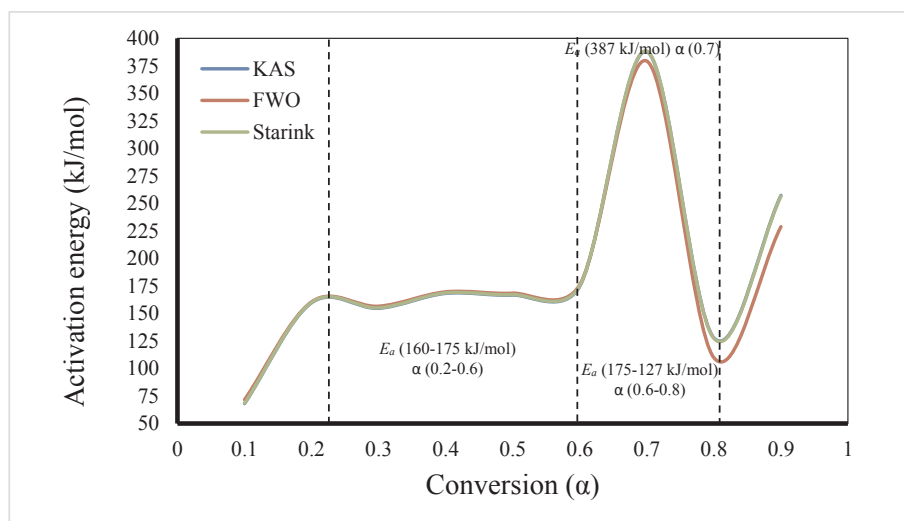


Fig. 3. Activation energy variation with conversion (α) for FWO, KAS and Starink Methods.

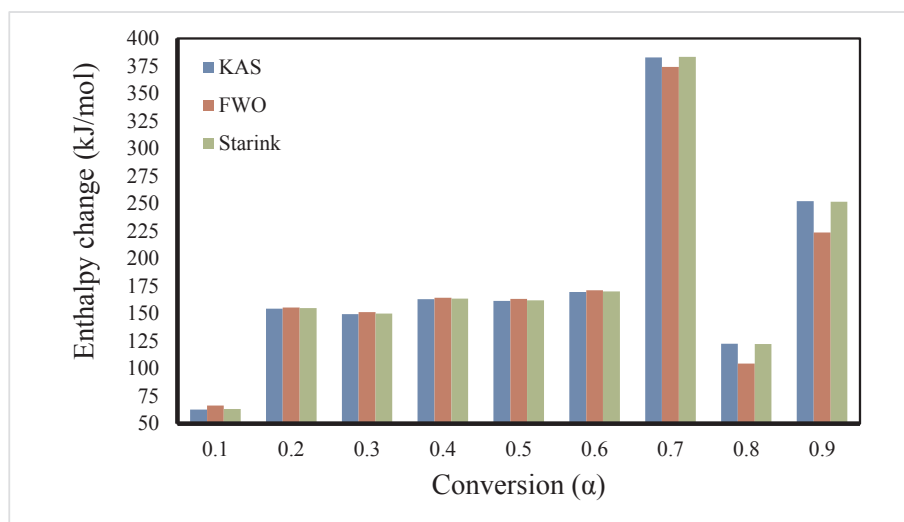


Fig. 4. Enthalpy variation with conversion (α) for FWO, KAS and Starink Methods.

(152–154 kJ/mol) and fermented corn stalks (88–172 kJ/mol) at the same conversional fractions [41,45]. So, it reflects the considerable bioenergy potential of JA biomass through pyrolysis.

3.4.4. Change in entropy (ΔS , J/mol)

The change in entropy is a direct reflection of the degree of disorder in the system in response to a certain set of varying conditions, which is the temperature in this case while it indicates the closeness of the system to its thermodynamic equilibrium. The ΔS values increased from -22 J/mol to 20 J/mol as conversional fraction varied from 0.2 to 0.6 with a peak rise at conversion 0.7 and later dropped at a higher conversional fraction. The negative values of ΔS indicate that sample was more organized at this stage as compared to the initial reaction state. Moreover, a wide range of changing entropy indicates complex reaction chemistry.

3.5. TG-FTIR-MS study to monitor the product formation

The IR spectrum obtained at peak temperature as observed in the DTG curve is shown in Fig. 5. An immense range of spectra is detected at 3400 – 4000 cm^{-1} wavenumber interval. These all spectra are related to stretching vibrations of hydroxyl vibrations i.e. O–H. They can be demonstrative of phenols, water or both compounds. Furthermore,

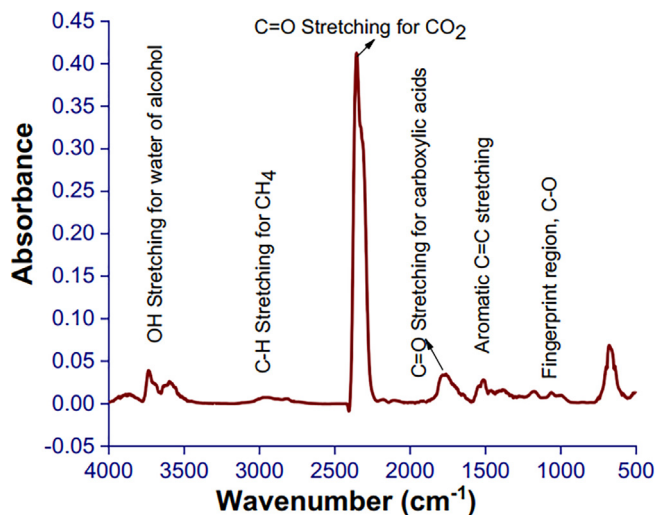


Fig. 5. FTIR Spectra of JA from wave number 500–4000.

from spectrums in fingerprint region, bending vibrations of O–H, hydroxyl group related to both compounds i.e. water (1505 cm^{-1} and 1750 cm^{-1}) and phenols (1336 cm^{-1} – 1450 cm^{-1}) are identified, confirming the presence of both water and phenols compounds in the evolved gas mixture during main stage of thermal decomposition. Previously, it was proposed [46] that phenols are initially produced due to dehydration of hydroxyl groups present in the alkyl side chain. Asymmetrical stretching for carbon dioxide occurs at about 2365 cm^{-1} [47], which is observed in FTIR analysis of evolved gas species. One of the sources to produce CO_2 is associated with carboxylic acids production which was confirmed by carbonyl band present at around 1708 cm^{-1} . Production of carbon dioxide from carboxylic acids takes place due to the decarboxylation reaction which means that most of the carboxylic acids produced in the evolved gas mixture were involved in carbon oxide production due to which a dominant amount of CO_2 is detected in FTIR spectrum. Earlier studies revealed that cracking of most thermolabile functional groups like carbonyl (C=O), carboxyl (COOH) and ether (R–O–R) contributed to CO_2 release [46]. Methane, CH_4 gas concentration (2850 – 2950 cm^{-1}) was found to be a very small fraction at this temperature. Many researchers suggested that the formation of methane gas takes place mainly due to fragmentation of side chains [46,48,49]. Furthermore, CH_4 formation is also a result of demethylation of methoxyl groups [50–52]. The band present at about 1500 cm^{-1} represent alkene formation. The formation of alkene might be associated with bond cleavage in ester with β -hydrogen and in cinnamyl diesters during pyrolysis. The ($\text{CH}_2 + \text{CH}_3$) decomposition associated with C–H functional groups also contributed to the formation of unsaturation at adjacent carbons. Alcohol was also detected in the FTIR spectrum at around 1052 cm^{-1} but in small concentration. There are two possibilities to produce alcohol during pyrolysis i.e. cracking of methoxy group and $-\text{CH}_2\text{OH}$ group in the side chain but in this present study, alcohol formation seems due to $-\text{CH}_2\text{OH}$ group in the side chain [46]. A small fraction of HCOOH (1173 cm^{-1}) was also detected.

Bands present at 1630 – 1780 in FTIR also showed the production of CH_3COOH . The intensity of C=O stretching representing CH_3COOH formation was found to be higher than HCOOH (1173 cm^{-1}) indicating that CH_3COOH formation is easier and abundant than HCOOH . While TG-MS further confirmed the presence of compounds having carbonyl and ester functional groups such as 3-Furaldehyde, Acetic acid, methyl ester, Acetic acid ethenyl ester, acetic acids, 3-Methyloxirane-2-carboxylic acid, Propanoic acid 2-oxo- methyl ester, 1,2-Ethanediol diacetate and 1,2-Epoxy-3-propyl acetate that were quite consistent with FTIR spectra. TG-FTIR analysis revealed the presence of all main

Table 4
TG-MS analyses of evolved gases during pyrolysis of JA biomass.

Sr. No	Compounds	Formulae	Molar masses	CAS No.
1	Toluene	C ₇ H ₈ O ₂	100.11	108-88-5
2	3-Furaldehyde	C ₅ H ₄ O ₂	96.08	498-60-2
3	1,2-Epoxy-3-propyl acetate	C ₅ H ₈ O ₃	116.15	6387-89-9
4	Acetic acid	C ₂ H ₄ O ₂	60	64-19-7
5	Acetic acid, methyl ester	C ₃ H ₆ O ₂	74.03	79-20-9
6	Acetic acid ethenyl ester	C ₄ H ₆ O ₂	86.08	108-05-4
7	3-Methyloxirane-2-carboxylic acid	C ₄ H ₆ O ₃	102.08	2443-40-5
8	Propanoic acid, 2-oxo-, methyl ester	C ₄ H ₆ O ₃	102.08	600-22-6
9	1,2-Ethanediole, diacetate	C ₆ H ₁₀ O ₄	146.41	111-55-7
10	Furan, 3-methyl-	C ₅ H ₆ O	82.10	930-27-8
11	2-Propanone, 1-hydroxy-	C ₁₈ H ₃₆ N ₄ O ₁₀	469	116-09-6
12	Cystine	C ₆ H ₁₂ N ₂ O ₄ S ₂	240.3	56-89-3
13	Pentanal	C ₅ H ₁₀ O	86.13	110-62-3
14	1,2-Epoxy-3-propyl acetate	C ₅ H ₈ O ₃	116.11	6387-89-9
15	1-Diphenylsilyloxyoctane	C ₂₀ H ₂₈ OSi	313	99221-40-6
16	Succindialdehyde	C ₄ H ₆ O ₂	86.08	638-37-9
17	Argon	Ar	39	7440-37-1
18	3-Furaldehyde	C ₅ H ₄ O ₂	96.08	498-60-2
19	3-Furanmethanol	C ₅ H ₆ O ₂	98.10	4412-91-3
20	4-Cyclopentene-1,3-diol, cis-	C ₅ H ₈ O ₂	100.11	29783-26-4
21	1,2,5-Oxadiazole	C ₂ H ₂ N ₂ O	70.05	288-37-9

gaseous compound which confirmed that thermal decomposition at peak temperature resulted in numerous gaseous products.

Around 21 compounds with their major derived components were detected through TG-MS as shown in Table 4. The TG-MS showed the abundance of ester groups, benzene and toluene rings that are the major energy generating groups that were also confirmed with the FTIR results. Production of these compounds demonstrated the capacity of JA biomass to yield an ample amount of energy upon pyrolysis.

4. Conclusion and prospects

The pyrolysis of Jerusalem artichoke (JA) is a three-stage reaction where most of the thermal transformation occurs at the temperature range of 270–430 °C followed by lignin degradation and char formation at the temperatures higher than 430 °C. The process can be optimized for industrial pyrolysis to produce energy, syngases, and biooil at this temperature range. Moreover, the range of activation energy values reflected the suitability of JA biomass for co-pyrolysis with other agricultural residual biomasses. The kinetics and thermodynamics data obtained through KAS, FWO, and Starink, methods were shown to be consistent with each other which can be used to simulate the pyrolysis of JA biomass on an industrial scale. The evolved gas analysis confirmed the release of high-energy compounds with ketone, aldehyde, aromatic and other functional groups. While the release of valuable chemicals including acetic acid and toluene reflected the potential of JA biomass for the lab-scale synthesis of these solvents. Overall, JA biomass showed to be a promising feedstock for energy and chemicals in energy efficient and environmentally sustainable manner.

Declaration of interests

The authors declare that they have no known competing financial interests or personal relationships that could have appeared to influence the work reported in this paper.

Acknowledgments

Authors are highly obliged to National Key R&D Program of China, Grant No. 2018YFB1501401 and National Natural Science Foundation of China for their financial support through NSFC Grant No.

21750110435.

References

- [1] Liao JC, Mi L, Pontrelli S, Luo S. Fuelling the future: microbial engineering for the production of sustainable biofuels. *Nat Rev Microbiol* 2016;14(5):288–304.
- [2] Mehmood MA, Ibrahim M, Rashid U, Nawaz M, Ali S, Hussain A, et al. Biomass production for bioenergy using marginal lands. *Sustainable Prod Consumpt* 2017;9:3–21.
- [3] Altintas MM, Eddy CK, Zhang M, McMillan JD, Kompala DS. Kinetic modeling to optimize pentose fermentation in *Zymomonas mobilis*. *Biotechnol Bioeng* 2006;94(2):273–95.
- [4] Onal E, Uzun BB, Putun AE. The effect of pyrolysis atmosphere on bio-oil yields and structure. *Int J Green Energy* 2017;14(1):1–8.
- [5] Fukuda S. Pyrolysis investigation for bio-oil production from various biomass feedstocks in Thailand. *Int J Green Energy* 2015;12(3):215–24.
- [6] Liu G, Liao Y, Guo S, Ma X, Zeng C, Wu J. Thermal behavior and kinetics of municipal solid waste during pyrolysis and combustion process. *Appl Therm Eng* 2016;98:400–8.
- [7] Ceylan S, Kazan D. Pyrolysis kinetics and thermal characteristics of microalgae *Nannochloropsis oculata* and *Tetraselmis* sp. *Bioresour Technol* 2015;187:1–5.
- [8] Maia AAD, de Moraes LC. Kinetic parameters of red pepper waste as biomass to solid biofuel. *Bioresour Technol* 2016;204:157–63.
- [9] Long Y, Ruan L, Lv X, Lv Y, Su J, Wen Y. TG-FTIR analysis of pyrolusite reduction by major biomass components. *Chin J Chem Eng* 2015;23(10):1691–7.
- [10] Ceylan S, Goldfarb JL. Green tide to green fuels: TG-FTIR analysis and kinetic study of *Ulva prolifera* pyrolysis. *Energy Convers Manage* 2015;101:263–70.
- [11] Dai M, Yu Z, Fang S, Ma X. Behaviors, product characteristics and kinetics of catalytic co-pyrolysis *Spirulina* and oil shale. *Energy Convers Manage* 2019;192:1–10.
- [12] Özsin G, Pütün AE. TGA/MS/FT-IR study for kinetic evaluation and evolved gas analysis of a biomass/PVC co-pyrolysis process. *Energy Convers Manage* 2019;182:143–53.
- [13] Heo HS, Park HJ, Park Y-K, Ryu C, Suh DJ, Suh Y-W, et al. Bio-oil production from fast pyrolysis of waste furniture sawdust in a fluidized bed. *Bioresour Technol* 2010;101(1):S91–6.
- [14] Braga RM, Melo DM, Aquino FM, Freitas JC, Melo MA, Barros JM, et al. Characterization and comparative study of pyrolysis kinetics of the rice husk and the elephant grass. *J Therm Anal Calorim* 2014;115(2):1915–20.
- [15] Wu W, Mei Y, Zhang L, Liu R, Cai J. Kinetics and reaction chemistry of pyrolysis and combustion of tobacco waste. *Fuel* 2015;156:71–80.
- [16] Rasool T, Srivastava VC, Khan M. Utilisation of a waste biomass, walnut shells, to produce bio-products via pyrolysis: investigation using ISO-conventional and neural network methods. *Biomass Convers Biorefin* 2018:1–11.
- [17] Müsellim E, Tahir MH, Ahmad MS, Ceylan S. Thermokinetic and TG/DSC-FTIR study of pea waste biomass pyrolysis. *Appl Therm Eng* 2018;137:54–61.
- [18] Ye G, Luo H, Ren Z, Ahmad MS, Liu C-G, Tawab A, et al. Evaluating the bioenergy potential of Chinese Liquor-industry waste through pyrolysis, thermogravimetric, kinetics and evolved gas analyses. *Energy Convers Manage* 2018;163:13–21.
- [19] Cai H, Liu J, Xie W, Kuo J, Buyukada M, Evrendilek F. Pyrolytic kinetics, reaction mechanisms and products of waste tea via TG-FTIR and Py-GC/MS. *Energy Convers Manage* 2019;184:436–47.
- [20] Tian B, Qiao Y, Bai L, Feng W, Jiang Y, Tian Y. Pyrolysis behavior and kinetics of the trapped small molecular phase in a lignite. *Energy Convers Manage* 2017;140:109–20.
- [21] Rogers J, Brammer J. Estimation of the production cost of fast pyrolysis bio-oil. *Biomass Bioenergy* 2012;36:208–17.
- [22] Li L, Wang G, Wang S, Qin S. Thermogravimetric and kinetic analysis of energy crop Jerusalem artichoke using the distributed activation energy model. *J Therm Anal Calorim* 2013;114(3):1183–9.
- [23] Ozawa T. A new method of analyzing thermogravimetric data. *Bull Chem Soc Jpn* 1965;38(11):1881–6.
- [24] Flynn JH, Wall LA. A quick, direct method for the determination of activation energy from thermogravimetric data. *J Polym Sci, Part C: Polym Lett* 1966;4(5):323–8.
- [25] Akahira T, Sunose T. Transactions of Joint Convention of Four Electrical Institutes (1969) 246.
- [26] Starink M. A new method for the derivation of activation energies from experiments performed at constant heating rate. *Thermochim Acta* 1996;288(1–2):97–104.
- [27] Vyazovkin S, Burnham AK, Criado JM, Pérez-Maqueada LA, Popescu C, Sbirrazzuoli N. ICTAC Kinetics Committee recommendations for performing kinetic computations on thermal analysis data. *Thermochim Acta* 2011;520(1–2):1–19.
- [28] Paulrud S, Nilsson C. Briquetting and combustion of spring-harvested reed canary-grass: effect of fuel composition. *Biomass Bioenergy* 2001;20(1):25–35.
- [29] Jeguirim M, Dorge S, Trouve G. Thermogravimetric analysis and emission characteristics of two energy crops in air atmosphere: *Arundo donax* and *Miscanthus giganteus*. *Bioresour Technol* 2010;101(2):788–93.
- [30] Ahmad MS, Mehmood MA, Al Ayed OS, Ye G, Luo H, Ibrahim M, et al. Kinetic analyses and pyrolytic behavior of Para grass (*Urochloa mutica*) for its bioenergy potential. *Bioresour Technol* 2017;224:708–13.
- [31] Mehmood MA, Ye G, Luo H, Liu C, Malik S, Afzal I, et al. Pyrolysis and kinetic analyses of Camel grass (*Cymbopogon schoenanthus*) for bioenergy. *Bioresour Technol* 2017;228:18–24.
- [32] Benavente V, Fullana A. Torrefaction of olive mill waste. *Biomass Bioenergy* 2015;73:186–94.
- [33] Bousdira K, Bousdira D, Bekkouche SMEA, Nouri LH, Legrand J. Kinetic pyrolysis

- study and classification of date palm biomass. *J Renewable Sustainable Energy* 2017;9(1):013102.
- [34] Demirbas A. Higher heating values of lignin types from wood and non-wood lignocellulosic biomasses. *Energy Sources Part A* 2017;39(6):592–8.
- [35] Balogun A, Lasode O, McDonald A. Devolatilisation kinetics and pyrolytic analyses of *Tectona grandis* [teak]. *Bioresour Technol* 2014;156:57–62.
- [36] Yang H, Yan R, Chin T, Liang DT, Chen H, Zheng C. Thermogravimetric analysis – Fourier transform infrared analysis of palm oil waste pyrolysis. *Energy Fuels* 2004;18(6):1814–21.
- [37] Gan DKW, Loy ACM, Chin BLF, Yusup S, Unrean P, Rianawati E, et al. Kinetics and thermodynamic analysis in one-pot pyrolysis of rice hull using renewable calcium oxide based catalysts. *Bioresour Technol* 2018.
- [38] Wang X, Hu M, Hu W, Chen Z, Liu S, Hu Z, et al. Thermogravimetric kinetic study of agricultural residue biomass pyrolysis based on combined kinetics. *Bioresour Technol* 2016;219:510–20.
- [39] Tahir MH, Çakman G, Goldfarb JL, Topcu Y, Naqvi SR, Ceylan S. Demonstrating the suitability of canola residue biomass to biofuel conversion via pyrolysis through reaction kinetics, thermodynamics and evolved gas analyses. *Bioresour Technol* 2019.
- [40] Tahir MH, Zhao Z, Ren J, Rasool T, Naqvi SR. Thermo-kinetics and gaseous product analysis of banana peel pyrolysis for its bioenergy potential. *Biomass Bioenergy* 2019;122:193–201.
- [41] Chong CT, Mong GR, Ng J-H, Chong WWF, Ani FN, Lam SS, et al. Pyrolysis characteristics and kinetic studies of horse manure using thermogravimetric analysis. *Energy Convers Manage* 2019;180:1260–7.
- [42] Yuan X, He T, Cao H, Yuan Q. Cattle manure pyrolysis process: kinetic and thermodynamic analysis with isoconversional methods. *Renewable Energy* 2017;107:489–96.
- [43] Ahmad MS, Mehmood MA, Taqvi STH, Elkamel A, Liu C-G, Xu J, et al. Pyrolysis, kinetics analysis, thermodynamics parameters and reaction mechanism of *Typha latifolia* to evaluate its bioenergy potential. *Bioresour Technol* 2017;245:491–501.
- [44] Ahmad MS, Mehmood MA, Liu C-G, Tawab A, Bai F-W, Sakdaronnarong C, et al. Bioenergy potential of *Wolfia arrhiza* appraised through pyrolysis, kinetics, thermodynamics parameters and TG-FTIR-MS study of the evolved gases. *Bioresour Technol* 2018;253:297–303.
- [45] He Y, Chang C, Li P, Han X, Li H, Fang S, et al. Thermal decomposition and kinetics of coal and fermented cornstalk using thermogravimetric analysis. *Bioresour Technol* 2018;259:294–303.
- [46] Wang S, Wang K, Liu Q, Gu Y, Luo Z, Cen K, et al. Comparison of the pyrolysis behavior of lignins from different tree species. *Biotechnol Adv* 2009;27(5):562–7.
- [47] Shokrlu YH, Maham Y, Tan X, Babadagli T, Gray M. Enhancement of the efficiency of in situ combustion technique for heavy-oil recovery by application of nickel ions. *Fuel* 2013;105:397–407.
- [48] Fu P, Yi W, Bai X, Li Z, Hu S, Xiang J. Effect of temperature on gas composition and char structural features of pyrolyzed agricultural residues. *Bioresour Technol* 2011;102(17):8211–9.
- [49] Xu C, Hu S, Xiang J, Zhang L, Sun L, Shuai C, et al. Interaction and kinetic analysis for coal and biomass co-gasification by TG-FTIR. *Bioresour Technol* 2014;154:313–21.
- [50] Cao J, Xiao G, Xu X, Shen D, Jin B. Study on carbonization of lignin by TG-FTIR and high-temperature carbonization reactor. *Fuel Process Technol* 2013;106:41–7.
- [51] Xu T, Huang X. Study on combustion mechanism of asphalt binder by using TG-FTIR technique. *Fuel* 2010;89(9):2185–90.
- [52] Luo Z, Wang S, Guo X. Selective pyrolysis of Organosolv lignin over zeolites with product analysis by TG-FTIR. *J Anal Appl Pyrol* 2012;95:112–7.